GEOPHYSICS, VOL. 73, NO. 6 (NOVEMBER-DECEMBER 2008); P. I43–I50, 5 FIGS., 1 TABLE.
10.1190/1.2976116

2D vector gravity potential and line integrals for the gravity anomaly caused by a 2D mass of depth-dependent density contrast

Xiaobing Zhou[1]

ABSTRACT

Using line integrals (LIs) used to calculate the gravity anomaly caused by a 2D mass of complicated geometry and spatially variable density contrast is a computationally efficient algorithm, that reduces the calculation from two dimensions to one dimension. This work has developed a mechanism for defining LIs systematically for different types of density functions. Two-dimensional vector gravity potential is defined as a vector, the net circulation of which, along the closed contour bounding a 2D mass, equals the gravity anomaly caused by the 2D mass. Two representative types of LIs are defined: an LI with an arctangent kernel for any depth-dependent density-contrast function, which has been studied historically; and an LI with a simple algebraic kernel for any integrable density-contrast function. The present work offers (1) a vectorial-based derivation of formulas that do not suffer from the arbitrary sign conventions found in some historical approaches; and (2) a simple algebraic kernel in line integrals as an alternative to the historical arctangent kernel, with the possibility of extension to more general cases. The concept of 2D vector gravity potential provides a useful tool for defining LIs systematically for any mass density function, helping us understand how dimensions can be reduced in a calculating gravity anomaly, especially when the density contrast varies with space. LIs have been tested in case studies. The maximum differences in calculated gravity anomalies by different LIs for the case studies were between 5.93×10^{-6} mGal and 3.52×10^{-11} mGal. Processing time required per station per segment of the 2D polygon of a 2D mass using LIs is 0.7–1.5 ms on a Dell Optiplex GX 620 desktop computer, almost independent of the density function. The results indicate that the two types of LIs provide very fast, efficient, and reliable algorithms in gravity modeling or inversion for various types of density-contrast functions.

INTRODUCTION

The success of inversion of alluvium thickness and basement relief in sedimentary basins, in which compaction plays an important role for groundwater assessment or petroleum exploration from gravity anomalies, greatly depends on the fidelity of the density model (Cordell, 1973; Hansen, 1999). Historically, based on the limited density data logged, quite a few density-contrast models have been proposed in gravity modeling. These models are categorized into two types: (1) the constant density-contrast model or average density-contrast model (e.g., Bott, 1960; Corbató, 1965; Ferguson, et al., 1988; Pohánka, 1988; Litinsky, 1989; Holstein and Ketteridge, 1996); and (2) the variable density-contrast model — the density contrast of sediments changes with depth and/or horizontal position partly as a result of compaction.

Variable density-contrast models include (1) exponential decay model (Cordell, 1973; Chai and Hinze, 1988; Litinsky, 1989; Chappell and Kusznir, 2008), (2) hyperbolic decay model (Litinsky, 1989; Silva et al., 2006), (3) linear model (Murthy and Rao, 1979; Pohánka, 1998; Hansen, 1999; Holstein, 2003), (4) quadratic model (Rao, 1986; Rao et al., 1990; García-Abdeslem et al., 2005), (5) parabolic model (Rao et al., 1994; Chakravarthi and Sundararajan, 2004), and (6) polynomial model (Guspí, 1990; Zhang et al., 2001).

Although historically the models for constant, linear, and quadratic density contrasts are described as models that differ from the polynomial model, they really are special cases of the polynomial model. The density contrast as a function of only depth is of great interest (Cordell, 1973; Murthy and Rao, 1979; Rao, 1986; Chai and Hinze, 1988; Litinsky, 1989; Rao et al., 1990; García-Abdeslem, 1992; Rao et al., 1994; Pohánka, 1998; Hansen, 1999; Holstein, 2003; García-Abdeslem et al., 2005; Silva et al., 2006; Chakravarthi and Sundararajan, 2007; Chappell and Kusznir, 2008). In the following discussion, I consider a density-contrast function that depends on only depth.

Inclusion of variable density contrast obviously introduces substantial complication not only in gravity modeling, but also in seismic modeling. For instance, if a mass target with spatially variable

Manuscript received by the Editor 24 February 2008; revised manuscript received 23 May 2008; published online 15 October 2008.
[1]Montana Tech of the University of Montana, Department of Geophysical Engineering, Butte, Montana, U.S.A. E-mail: xzhou@mtech.edu.
© 2008 Society of Exploration Geophysicists. All rights reserved.

density is modeled as two or more bodies with different constant densities, the density contrast across the interface introduces spurious reflections (Hansen, 1999; Holstein, 2003). However, inclusion of the variable density contrast does approach more real gravity problems.

In general, obtaining an analytic expression for the gravity anomaly caused by an inhomogeneous mass body of complex shape often is not possible. Thus, numerical calculation often is inevitable. For efficient numerical calculation, dimension reduction by transforming 2D areal integrals into 1D always should be a goal. The objectives of this work are (1) to investigate systematically the mechanism of forming LIs to realize dimension reduction; and (2) to find representative types of LIs for different types of density-contrast functions so that these LIs can provide very fast, efficient, and reliable algorithms in gravity modeling or inversion.

In the next section, I start from Newton's gravitational law, Stoke's theorem, and the right-hand rule to define the 2D vector gravity potential, so that transformation of the 2D areal integral for a 2D mass to 1D LIs can be performed from a mathematically rigorous viewpoint. I discuss the nonuniqueness of the 2D vector gravity potential. Then I derive the LIs with arctangent kernel with integration direction determined solely by the right-hand rule. I discuss agreement with, and improvement upon, the historical LIs of the literature. In the subsequent section, I derive the LIs with a simple algebraic kernel for any integrable density-contrast function of depth. Then I show the accuracy and computation time requirement using the two types of LIs in case studies. Discussion and conclusions are given in the last section.

2D VECTOR GRAVITY POTENTIAL

Consider the geometry shown in Figure 1. An infinitesimal mass difference $dm = \Delta\rho dV$ between a 2D mass and its background is at point (x,y,z), where $\Delta\rho$ is the density contrast, dV is the infinitesimal volume, and the observation point is on the surface at point $P(x_i,0,0)$. From Newton's law, the magnitude of attraction on a unit mass at point P resulting from the infinitesimal mass dm at distance r is given by

$$d\mathbf{F} = G\frac{dm}{r^2}\hat{\mathbf{r}} = G\frac{\Delta\rho dV}{r^2}\hat{\mathbf{r}}, \tag{1}$$

where G is the Newton's gravitational constant, r is the distance between the observation point and the mass source $dm = \Delta\rho dV$, and $\hat{\mathbf{r}}$ is the unit vector in the direction from the observation point to the mass source.

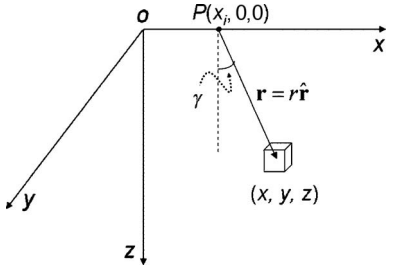

Figure 1. A scheme demonstrating the gravity at an observation point $P(x_i,0,0)$ on the earth's surface along the x-axis resulting from a mass element at source point (x,y,z).

The vertical component of gravity observed at point $P(x_i,0,0)$ is

$$g_z(x_i,0,0) = G\int_V\oint\frac{\Delta\rho dV}{r^2}\hat{\mathbf{z}}\cdot\hat{\mathbf{r}} = G\int_V\oint\frac{\Delta\rho z dy dx dz}{\sqrt{[(x-x_i)^2+y^2+z^2]^3}}, \tag{2}$$

where $\hat{\mathbf{z}}$ is the unit vector in z-direction (Figure 1). Assume the mass source is infinite in the y-direction, and the density contrast is assumed to be independent of y. Carrying out the integration with respect to y from $-L_y$ to $+L_y$ as $L_y\to\infty$ yields

$$g_z(x_i,0,0) = \lim_{L_y\to\infty} G\int_S\oint\Delta\rho(z)z dx dz, \tag{3}$$

where S is the area projected onto the xz-plane.

Let us denote

$$I_1 = \lim_{L_y\to\infty}\int_{-L_y}^{L_y}\frac{dy}{\sqrt{[(x-x_i)^2+y^2+z^2]^3}} = \frac{2}{(x-x_i)^2+z^2}. \tag{4}$$

Thus, for an arbitrary 2D mass body in the x-z plane ($y = 0$), the vertical component of gravity at point $P(x_i,0)$ is

$$g_z(x_i,0) = 2G\int_S\oint\frac{\Delta\rho(z)z}{(x-x_i)^2+z^2}dx dz. \tag{5}$$

This is the general form of the 2D areal integral for calculating gravity anomaly at any point $P(x_i,0)$ in the x-z plane caused by 2D masses with density contrast variable in depth z.

To convert the 2D areal integral (equation 5) to 1D LI, I resort to Stoke's theorem,

$$\int_S(\nabla\times\mathbf{A})\cdot d\mathbf{s} = \oint_C\mathbf{A}\cdot d\mathbf{l}, \tag{6}$$

where $\mathbf{A}$ is an arbitrary vector, $d\mathbf{s}$ is a differential areal vector, and $d\mathbf{l}$ is a differential length along the contour C bounding the surface S. The direction of $d\mathbf{s}$ and that of $d\mathbf{l}$ must satisfy the right-hand rule; i.e., when curling the fingers of the right hand along the direction of $d\mathbf{l}$, the thumb points to the direction of $d\mathbf{s}$. This is the basis for determining the integration direction along the contour bounding the area S in the LI of the right-hand side (RHS) of equation 6.

In the x-z plane as shown in Figure 2, I choose

$$d\mathbf{s} = \hat{\mathbf{y}}dx dz; \tag{7}$$

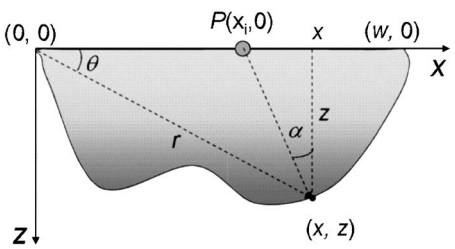

Figure 2. The 2D cross section of a sedimentary basin with density contrast increasing with depth. Width of the basin is w.

i.e., the direction of $d\mathbf{s}$ is along the positive y-axis (unit vector $\hat{\mathbf{y}}$). From the right-hand rule, the direction of $d\mathbf{l}$ along the contour bounding the area as shown in Figure 2 is counterclockwise; i.e.,

$$d\mathbf{l} = \hat{\mathbf{x}}dx + \hat{\mathbf{z}}dz. \quad (8)$$

Equation 6 becomes

$$\int_S (\nabla \times \mathbf{A}) \cdot d\mathbf{s} = \iint_S \left(\frac{\partial A_x}{\partial z} - \frac{\partial A_z}{\partial x} \right) dxdz$$

$$= \oint_C (A_x dx + A_z dz). \quad (9)$$

where notation $\oint_C$ denotes the line integration counterclockwise along the contour C of the 2D mass (Figure 2). Similarly, $\oint_C$ denotes the line integration clockwise along the contour C.

Comparing equation 9 with equation 5, if I want to convert an areal integral for gravity (RHS of equation 5) to an LI (RHS of equation 9), I need only to find a vector $\mathbf{A}$ satisfying

$$\frac{\partial A_x}{\partial z} - \frac{\partial A_z}{\partial x} = \frac{2G\Delta\rho(z)z}{(x - x_i)^2 + z^2}, \quad (10)$$

so that the gravity anomaly caused by a 2D mass becomes

$$g(x_i,0) = \oint_C (A_x dx + A_z dz). \quad (11)$$

I define the vector $\mathbf{A}$ that satisfies equation 10 as the 2D vector gravity potential, so that the gravity anomaly caused by a 2D mass equals the net circulation of the 2D vector gravity potential along the closed contour bounding the mass.

Equation 11 is derived based on the choice that the direction of the differential area is along the positive direction of y-axis. If I choose the negative direction of y-axis as the direction of $ds = dxdz$, direction of the line element should be $d\mathbf{l} = -\hat{\mathbf{x}}dx - \hat{\mathbf{z}}dz$, corresponding to the clockwise direction along the contour in Figure 2. The gravity anomaly then is

$$g(x_i,0) = -\oint_C (A_x dx + A_z dz). \quad (12)$$

Because changing integration direction results only in the sign change of the integral, I consider only anticlockwise integration. Thus, the default line integration is $\oint_C$ in the following discussion.

Because the curl of the gradient of any scalar field is identically zero, i.e., for any scalar field $V(x,z)$, $\nabla \times (\nabla V) = 0$, I have

$$\nabla \times \mathbf{A} = \nabla \times (\mathbf{A} + \nabla V). \quad (13)$$

This means that the 2D vector gravity potential defined by equation 10 is not unique; but the gravity anomaly calculated by various 2D vector gravity potentials satisfying equation 10 should be exactly the same, as determined by equation 11 and 12. This nonuniqueness of the 2D vector gravity potential, but uniqueness of the gravity anomaly, provides many options for gravity anomaly calculation using LI equations 11 and 12 through selecting different 2D vector gravity potentials ($\mathbf{A}$'s) for different forms of density-contrast function.

LINE INTEGRALS WITH ARCTANGENT KERNEL

The nonuniqueness of 2D vector gravity allows me to choose the $\mathbf{A}$ that satisfies equation 10. In this section, I derive the LIs with arctangent kernel and compare them with historical LIs when the density-contrast function is dependent only on depth.

Let us choose the 2D vector gravity potential $\mathbf{A}$ that satisfies equation 10 as follows:

$$A_x = 0,$$

$$A_z = -2G\Delta\rho(z)z \oint_C \frac{dx}{(x - x_i)^2 + z^2} \quad (14)$$

$$= -2G\Delta\rho(z)\arctan\left(\oint_C \frac{x - x_i}{z} \right).$$

Inserting equation 14 in equation 11, the vertical component of gravity anomaly becomes

$$g_z(x_i,0) = \oint_C \mathbf{A} \cdot d\mathbf{l} = -2G \oint_C \Delta\rho(z)\arctan\left(\oint_C \frac{x - x_i}{z} \right) dz$$

$$= -2G \oint_C \Delta\rho(z)\alpha dz, \quad (15)$$

where $\alpha = \alpha(x - x_i, z)$ is the angle between the line connecting the observation point to the source and the vertical line at the source (Figure 2). This indicates that for the density-contrast model $\Delta\rho(z)$ I can choose a 2D vector gravity potential $\mathbf{A}$ as given in equation 14; so that the vertical component of gravity anomaly caused by a 2D mass body is equal to the net circulation of the 2D vector gravity potential $\mathbf{A}$ around the closed contour bounding the 2D mass body.

Because the 2D vector gravity potential (equation 14) is dependent on an arctangent function for depth-dependent density-contrast functions, and thus the gravity anomaly is calculated by LIs with arctangent kernel, LI (equation 15) is referred to as LI with arctangent kernel to differentiate it from the other type of LI for integrable density-contrast function to be discussed.

Historical integrals with arctangent kernel for constant density-contrast model

Consider the case when the density contrast of the 2D mass is a constant; i.e., $\Delta\rho(z) = \Delta\rho_0$. At the origin of the coordinate system ($x_i = 0$), the vertical component of the gravity anomaly from the LI of arctangent kernel (equation 15) becomes

$$g_z(0,0) = -2G\Delta\rho_0 \oint_C \arctan\left(\oint_C \frac{x}{z} \right) dz$$

$$= -2G\Delta\rho_0 \oint_C \left(\frac{\pi\theta}{2} - \right) dz = 2G\Delta\rho_0 \oint_C \oint_C dz. \quad (16)$$

Because

$$\oint_C dz = z \oint_C - \oint_C zd = 0 - \oint_C zd = -\oint_C zd, \quad (17)$$

it yields

$$g_z(0,0)_\oint = 2G\Delta\rho_0 \oint_C dz = -2G\Delta\rho_0 \iint_\sigma d\quad . \quad (18)$$

Comparison with historical line integrals

Consider again the 2D geometry of a mass body as shown in Figure 2. Hubbert (1948) showed that the vertical component of the gravity anomaly at the origin (0, 0) of coordinates by a 2D mass of constant density contrast $\Delta\rho_0$ can be calculated by the LI

$$g_z(0,0)_\oint = 2G\Delta\rho_0 \quad dz = -2G\Delta\rho_0 \quad zd\ , \quad (19)_\oint$$

where is the polar angle between r and the horizontal x-axis. Hubbert's LI (equation 19) later became the basis for the classic Talwani et al. (1959) computational scheme for rapid computation of gravity caused by 2D masses when the mass density is constant.

In Hubbert's paper, the direction of the integration for the LI along the contour bounding the mass (contour line in Figure 2) was not specified systematically. However, Figure 4 in Hubbert's paper did indicate that the integration direction of Hubbert's LI (equation 19) is counterclockwise. Comparing equation 18 with equation 19, it is easy to see that they are exactly the same. Therefore, I conclude that the general LI (equation 15) with **A** given by equation 14 degenerates to Hubbert's LI when the density contrast is constant and the observation point is at the origin.

Murthy and Rao (1979) extrapolated Hubbert's LI for the case of constant density contrast to the case that the mass density contrast varies with depth as

$$\begin{aligned} g_z(0,0)_\oint &= -2G \quad \Delta\rho(z)_\oint\, dz \\ &= -2G \quad \Delta\rho(z)\arctan\left(\oint_x dz. \right. \end{aligned} \quad (20)_\oint$$

Murthy and Rao (1979) stated that the line integration is carried out in the clockwise direction along the contour bounding the mass. The change of sign with change of direction of the contour is well understood, but standard conventions were not always followed in the past.

From equation 15, but for clockwise integration, the gravity anomaly at the origin is

$$\begin{aligned} g_z(0,0)_\oint &= 2G\oint_C \Delta\rho(z)\arctan\left(\oint_x dz \right. \\ &= 2G\oint_C \Delta\rho(z)\left(\oint \frac{\pi\theta}{2} - \arctan\left(\oint_x \right. \right. \quad dz \\ &= -2G\oint_C \Delta\rho(z)_\oint\, dz, \end{aligned} \quad (21)_\oint$$

which is the same as the LI of Murthy and Rao (1979). However, here for each form of the LI (equations 15 and 18), the associated integration direction along the contour bounding the 2D mass is specified uniquely based on the right-hand rule; therefore, the LIs do not suffer from arbitrary sign conventions. This is an improvement compared with the original development of the LIs by Hubbert (1948) and Murthy and Rao (1979), whereby the integration direction for the LI was not defined systematically.

The above comparison with the historical LIs (for only constant or depth-dependent density-contrast functions) shows that the line integrals with arctangent kernel (equations 15 and 18) degenerate to the historical LIs of the literature when the conditions for these historical LIs are satisfied, and when direction of the integration along the contour is followed well. For calculating the gravity anomaly at observation points not at the origin, I suggest using equation 15 so that the integrand and equation of the contour (the boundary of the 2D mass) need not be transformed for calculation at each observation point.

DENSITY-INTEGRATED LINE INTEGRALS FOR ANY INTEGRABLE DENSITY-CONTRAST FUNCTION

Now let us find the LIs when the density-contrast function is integrable. Let me define the density-contrast integral as

$$F(z)_\oint = \int \Delta\rho(z)dz + C_0, \quad (22)_\oint$$

where C_0 is a constant that is independent of z for a specific density-contrast model. It can be readily proved that

$$\begin{aligned} &\frac{\partial}{\partial z}\left[\frac{2GF(z)z}{(x-x_i)^2+z^2}\right] + \frac{\partial}{\partial x}\left[\oint \frac{G(x-x_i)F(z)}{(x-x_i)^2+z^2}\right] \\ &\quad = \frac{2G\Delta\rho(z)z}{(x-x_i)^2+z^2}. \end{aligned} \quad (23)$$

Comparing equation 23 with equation 10, I can define a 2D vector gravity potential as

$$\begin{aligned} A_x &= 2G\frac{F(z)z}{(x-x_i)^2+z^2}, \\ A_z &= -2G\frac{(x-x_i)F(z)_\oint}{(x-x_i)^2+z^2}. \end{aligned} \quad (24)$$

Inserting equation 24 in equation 11, the LIs for the gravity anomaly caused by a 2D mass become

$$\begin{aligned} g(x_i,0)_\oint = 2G\left(\iint_\sigma \frac{F(z)z}{(x-x_i)^2+z^2}dx \right. \\ \left. - \oint_C \frac{(x-x_i)F(z)_\oint}{(x-x_i)^2+z^2}dz \right. \end{aligned} \quad (25)$$

For numerical calculation, z in the first integral in equation 25 should be expressed as a function of x, whereas x in the second integral

should be expressed as a function of z using the equation of the contour or the equation of each segment of the contour. However, for a specific density-contrast model, the constant C_0 in equation 22 must be determined.

Calculation of C_0 depends on the properties of F(z); and $F(z)\oint$ should satisfy the condition that $F(z)|_{z=0} = 0$, because the gravity anomaly is zero when the thickness in z-direction of the mass body approaches zero for any density-contrast model, or when the density contrast is zero for any thickness of the mass body. This physical condition is used to find C_0 for a specific density-contrast model. For the constant density-contrast model, i.e., $\Delta\rho(z)\oint = \Delta\rho_0$, $C_0 = 0$. The density-contrast integral is $F(z)\oint = \Delta\rho_0 z$. Thus, for any integrable density-contrast function, the vertical component of gravity anomaly caused by a 2D mass body is equal to the net circulation of the 2D vector gravity potential **A** given by equation 24 around the closed contour bounding the 2D mass body. Because the 2D vector gravity potential given in equation 24 involves the integral of the density-contrast function (equation 22), the LIs given by equations 11 and 12 with **A** given by equation 24 are called density-integrated LIs with algebraic kernel.

In the above derivation of LI with algebraic kernel (equation 25), I implicitly assume that the observation station is outside the mass body. When the observation station is inside the mass body, equation 25 still holds. When this happens, the Cauchy integral formula or residue theorem must be used to evaluate the contour integrals in equation 25. Therefore, the line integral (equation 25) is valid for an observation point either inside or outside the target.

CASE STUDIES OF ACCURACY AND CPU TIME REQUIREMENT OF LINE INTEGRALS

For the depth-dependent density-contrast model, the gravity anomaly for a 2D mass body can be calculated by the LI with arctangent kernel given by equation 15. If the density-contrast function is integrable, the density-integrated LI (equation 25) can be used.

Consider the gravity anomaly along a transect on the x-axis caused by a polygon 2D mass shown in Figure 3 (top). The density contrast is assumed to depend on z quadratically as in the Sebastián Vizcaíno Basin, Mexico (García-Abdeslem et al., 2005); thus

$$\Delta\rho(z)\oint = -0.7 + 2.548 \times 10^{-4} z - 2.73 \times 10^{-8} z^2, \quad (26)\oint$$

where $\Delta\rho(z)\oint$ is in g/cm^3, and z in m. Because only the integral is concerned, the Gauss-Legendre quadrature method (Zhou et al., 2003) was used to carry out the integrations of equations 15 and 25. Because the abscissas and weights of the n-point Gauss-Legendre quadrature formula are based on the interval $(-1,1)$, the actual integration interval for each segment of the polygonal cross section is transformed into the $(-1,1)\oint$ range (Davis and Rabinowitz, 1984).

For the LI with arctangent kernel (equation 15), the density-contrast function can be inserted in the integral directly. For the density-integrated LI with algebraic kernel (equation 25), if we insert the quadratic-density-contrast model in equation 22, the density-contrast integral takes the form

$$F(z)\oint = \int \Delta\rho(z)dz = -0.7z + 1.274 \times 10^{-4} z^2 - 9.1 \times 10^{-9} z^3, \quad (27)\oint$$

where constant C_0 in equation 22 is found to be zero because $F(z)\oint$ satisfies $F(z)|_{z=0} = 0$.

By inserting equation 27 in equation 24, the 2D vector gravity potential takes the form

$$A_x = 2G\frac{(-0.7 + 1.274 \times 10^{-4} z - 9.1 \times 10^{-9} z^2) z^2}{(x - x_i)^2 + z^2},$$
$$A_z = 2G\frac{(0.7 - 1.274 \times 10^{-4} z + 9.1 \times 10^{-9} z^2)(x - x_i) z.}{(x - x_i)^2 + z^2} \quad (28)\oint$$

The contour usually is approximated as a polygon, with each segment or side of the polygon being a line segment, unless the exact form of the contour equation is known. The number of vertices or segments of the contour bounding the mass is assumed to be M (for Figure 3, $M = 7$).

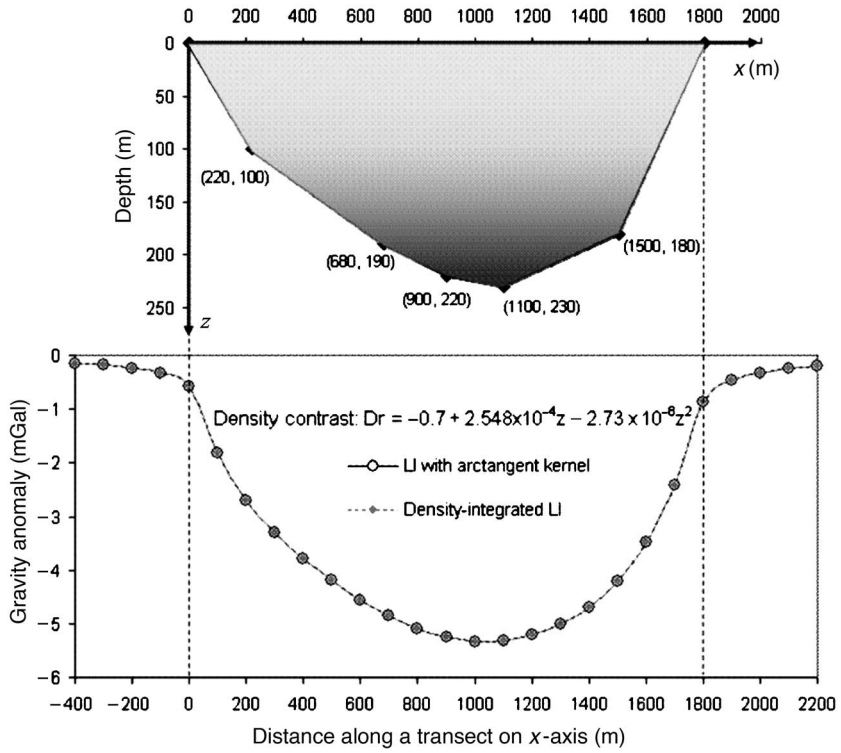

Figure 3. Top: Polygon contour of a 2D mass, length unit m. It is a model representing the 2D cross section of an elongated sediment valley with sedimentary density contrast represented by a quadratic model $\Delta\rho(z)\oint = -0.7 + 2.548 \times 10^{-4} z - 2.73 \times 10^{-8} z^2$ g/cm^3, where z is in m. Bottom: Gravity anomalies calculated using the LI with arctangent kernel (equation 15) and density-integrated LI (equation 25).

The kth segment is formed from points (x_k, z_k) and (x_{k+1}, z_{k+1}) in counterclockwise order, whose line equation is given in parametric form (H. Holstein, personal communication, 2008),

$$x = x_k(1 - t) + x_{k+1}t, \quad z = z_k(1 - t) + z_{k+1}t \tag{29}$$

and

$$dx = (x_{k+1} - x_k)dt, \quad dz = (z_{k+1} - z_k)dt, \tag{30}$$

where t is a parameter between 0 and 1.

This parameterized form for the mass boundary has the added advantage that the interval [0, 1] for t is adapted easily for Gaussian quadrature. Thus, equation 15 becomes

$$g_z(x_i, 0) = -2G\sum_{k=1}^{M}\int_{z_k}^{z_{k+1}}\Delta\rho(z)\arctan\left(\frac{x - x_i}{z}\right)dz, \tag{31}$$

and equation 25 becomes

$$g_z(x_i, 0) = \sum_{k=1}^{M}\left(\int_{x_k}^{x_{k+1}} A_x dx + \int_{z_k}^{z_{k+1}} A_z dz\right) \tag{32}$$

For the quadratic-density-contrast model (equation 26), the two components of the 2D vector gravity potential in equation 32 are given in equation 28.

Figure 3 (top) shows the shaded geometry of a sedimentary basin with density contrast decreasing with depth (equation 26). Figure 3 (bottom) shows the numerical solutions of equations 31 and 32 for the gravity anomaly along a transect with 27 observation stations on x-axis using the Gauss-Legendre method. The maximum difference between the gravity anomalies calculated using the LI with arctangent kernel (equation 31) and the LI with algebraic kernel (equation 32) is 3.52×10^{-11} mGal when $n = 10$, where n is the number of nodes for Gaussian quadrature. That maximum difference is 1.11×10^{-15} mGal when $n = 30$. When $n = 10$, calculation at the 27 points in Figure 3 (bottom) using equations 31 and 32 requires about 64 ms and 130 ms, respectively, on a Dell Optiplex GX 620 desktop computer. When $n = 30$, calculation using equations 31 and 32 requires about 143 ms and 277 ms, respectively, on the same computer.

The maximum difference between $n = 30$ and $n = 10$ in the calculated gravity anomalies at the 27 stations in Figure 3, using equation 31, is 3.52×10^{-11} mGal. This indicates that the improvement in the calculated results from the increase in the number of nodes from 10 through 30 in Gaussian quadrature is slim, although CPU time increases more than double. For most cases, $n = 10$ might be good enough.

Figure 4 shows the comparison of the gravity anomaly of a sedimentary valley (approximated as a polygon) calculated using the LIs with Zhang's modeling results (Zhang, 2001). The thickness at the center of the valley is 2 km, and the width of the sedimentary basin is 10 km. The density contrast is assumed to depend on z linearly (Zhang et al., 2001); thus

$$\Delta\rho(z) = -0.55 + 2 \times 10^{-4}z, \tag{33}$$

where $\Delta\rho(z)$ is in g/cm^3, and z in m. Results using the LIs developed in this work agree well with those of Zhang et al. (2001).

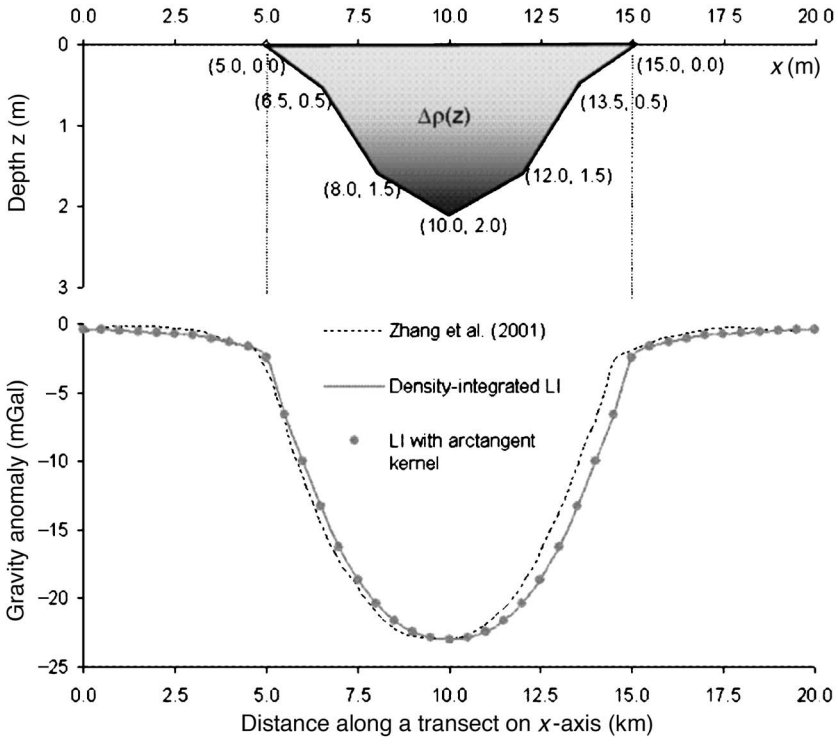

Figure 4. Top: Polygon contour of a 2D mass, representing the 2D cross section of an elongated sediment valley. Bottom: Gravity anomalies using the LI with arctangent kernel (equation 15), density-integrated LI (equation 25), and results by Zhang et al. (2001).

Figure 5 shows the gravity anomaly of a 2D basin approximated as a 2D polygon with density contrast being an exponential function (Chai and Hinze, 1988),

$$\Delta\rho(z) = -0.5\exp(-1.609 \times 10^{-4}z), \tag{34}$$

where $\Delta\rho(z)$ is in g/cm^3, and z in m. The density-contrast integral is

$$F(z) = \int \Delta\rho(z)dz + C_0 = -6224.04\exp(-0.8045 \times 10^{-4}z)\sinh(0.8045 \times 10^{-4}z), \tag{35}$$

where the constant C_0 in equation 22 is found to be 3107.52 m·g/cm^3. Gravity anomalies are calculated by the LI with the arctangent kernel (equation 31) and density-integrated LI with algebraic kernel (equation 32).

Results of Chai and Hinze (1988) also are shown in Figure 5 for comparison. The contour of the basin is approximated by a 142-segment polygon. The gravity anomalies are calculated for a total of 128 observation stations. The number of nodes for Gaussian quadrature is $n = 30$. The maximum difference between the gravity anoma-

lies calculated by equation 31 and by equation 32 is 5.93 $\times 10^{-6}$ mGal, which indicates that both methods agree very well with each other. However, the magnitude of the gravity anomalies calculated by Chai and Hinze (1988) is larger than that calculated by both methods developed here.

Calculation for the 128 stations using the LIs requires about 13.501 s CPU time and 25.754 s CPU time, respectively, on the Dell Optiplex GX 620 desktop computer. CPU time required per station per segment using these LIs for the exponential density-contrast model is 0.74–1.50 ms, almost equal to that for the second order polynomial density-contrast model, which is 0.77–1.54 ms. Table 1 summarizes CPU time and maximum difference in gravity anomalies $\Delta g_{z,\max}$ calculated using the two types of LIs in application to the quadratic and exponential density-contrast models. Results indicate that the CPU time required to calculate gravity anomalies using these LIs is similar and almost independent of the density-contrast model, but dependent on the complexity of geometry.

DISCUSSION

Converting 2D areal integrals to 1D line integrals in computing a gravity anomalies caused by 2D masses of complicated geometry and spatially variable density is efficient because the calculation is reduced to one dimension from two dimensions. Based on Newton's gravitational law, Stoke's theorem, and the right-hand rule, a systematic study from a mathematically rigorous viewpoint was made of LIs for calculating gravity anomalies caused by 2D masses of depth-dependent density contrast and the associated integration direction along the contour bounding the 2D masses.

Based on Stoke's theorem, I defined the 2D vector gravity potential as a vector so that the gravity anomaly caused by a 2D mass of variable density contrast is equal to the net circulation of the 2D vector gravity potential along the closed contour bounding the mass. The 2D vector gravity potential for a specific problem is not unique. This nonuniqueness of the 2D vector gravity potential, and the uniqueness of the gravity anomaly calculated, provide possibilities of defining LIs for calculating gravity anomalies caused by 2D masses of various forms of density-contrast functions.

By appropriately choosing the 2D vector gravity potential that satisfies Stoke's theorem when applied to conversion from areal integrals to line integrals for gravity anomaly computation, I defined two representative types of LIs based on forms of density-contrast functions: (1) LIs with the arctangent kernel that apply to any depth-dependent density-contrast function; and (2) density-integrated LIs with the algebraic kernel that apply to any density-contrast function that is integrable (e.g., exponential and polynomial density-contrast models). The LIs with the arctangent kernel degenerate to Hubbert's (1948) LI for the constant-density case and Murthy and Rao's (1979) LI for depth-dependent density contrast when calculating the gravity at the origin in a clockwise direction. Numerical case studies using

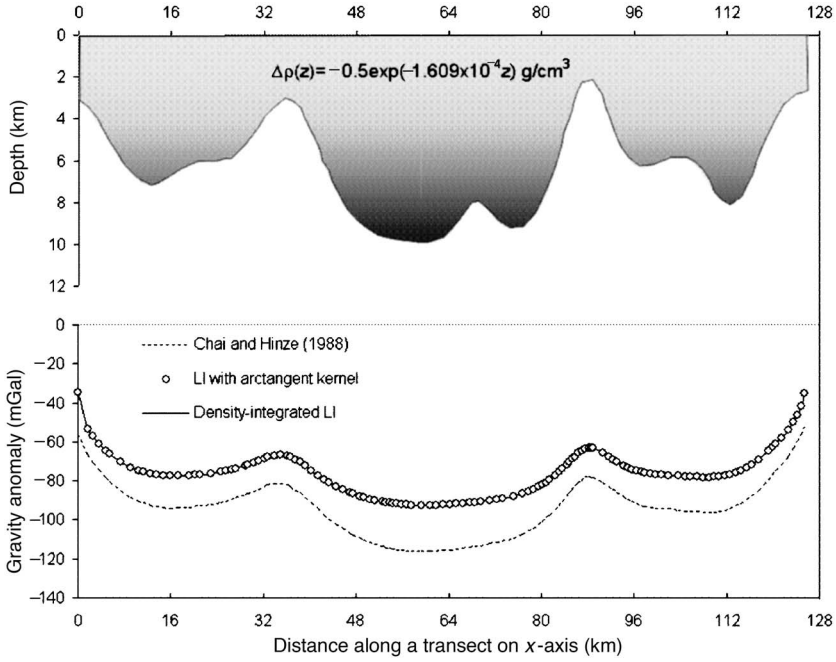

Figure 5. Top: Polygon contour of a 2D basin with sedimentary density contrast represented by an exponential decay model $\Delta\rho(z)\natural = -0.5\exp(-1.609\times10^{-4}z)\natural$ g/cm^3, where z is in m. Bottom: Gravity anomalies calculated using the LI with arctangent kernel (equation 15), density-integrated LI (equation 25), and results by Chai and Hinze (1988).

Table 1. Comparison of LIs in gravity-anomaly calculation for quadratic and exponential density-contrast models. LI/arc and LI/alg refer to LI with arctangent kernel and LI with algebraic kernel, respectively.

Density-contrast model		Quadratic		Exponential
Nodes $(n)\natural$ of Gaussian quadrature		10	30	30
Segments $(M)\natural$		7	7	142
Stations		27	27	128
$\Delta g_{z,\max}$ between LI/arc and LI/alg (mGal)		3.52×10^{-11}	1.11×10^{-15}	5.93×10^{-6}
CPU	LI/arc	64 ms	130 ms	13.501 s
	LI/alg	143 ms	277 ms	25.754 s
CPU/station/segment		—	0.74–1.50 ms	0.77–1.54 ms

the polynomial density-contrast model (linear model and quadratic model as two special cases) and exponential density-contrast model were carried out, and CPU time was monitored for each type of LI. Results show that CPU times required by the LIs are of the same order (0.7–1.5 ms per station per segment).

When the density contrast is assumed to be dependent on only depth, LIs with the arctangent kernel can be established. If the density contrast is dependent on only, or also on, horizontal position (x) in the cross sectional plane, LIs with the arctangent kernel do not exist. However, using the technique of 2D vector gravity potential, reduction of the anomaly evaluation to line integral evaluation still might be possible for some density functions that vary both horizontally and vertically in the cross-sectional plane of the mass body. Therefore, using the 2D vector gravity potential provides a useful tool in converting 2D areal integrals to 1D line integrals for accurate and fast gravity anomaly computation for any possible density-contrast model.

CONCLUSIONS

Based on Stoke's theorem, the concept of 2D vector gravity potential is defined. The gravity anomaly caused by a 2D mass of variable density contrast is equal to the net circulation of the 2D vector gravity potential along the closed contour bounding the mass. In converting 2D areal integrals to 1D line integrals for calculating gravity anomaly caused by 2D masses, the concept of a 2D vector gravity potential and its nonuniqueness provides a useful tool in defining systematically the LIs for any mass density function, helping us understand how dimensions can be reduced in calculating gravity anomalies. The integration direction in the LIs is specified uniquely by the right-hand rule so that the LIs do not suffer from arbitrary sign conventions found in some historical approaches.

Two representative types of LIs were established based on different forms of density functions, LIs with an arctangent kernel and density-integrated LIs with a simple algebraic kernel. CPU time required per station per segment of the 2D polygon of a 2D mass using the LIs is 0.7-1.5 ms, almost independent of density function. This indicates that the LIs are computationally very efficient and parsimonious in calculating gravity anomaly. The maximum differences in calculated gravity anomalies by different LIs for the case studies are between 5.93×10^{-6} mGal and 3.52×10^{-11} mGal. These results show that the two types of LIs provide very fast, efficient, and reliable algorithms in gravity modeling or inversion for various types of density-contrast functions.

ACKNOWLEDGMENTS

I am very grateful to Horst Holstein for his meticulous review of the manuscript. His very insightful, constructive, and helpful comments and suggestions greatly improve the quality of the manuscript. Sincere thanks go also to Marvin Speece (Montana Tech); Curtis Link (Montana Tech); Rao Yalamanchili, reviewer; John Peirce, associate editor; José M. Carcione, assistant editor; and Kees Wapenaar, editor; for their review and very useful comments and suggestions.

REFERENCES

Bott, M. H. P., 1960, The use of rapid digital computing methods for direct gravity interpretation of sedimentary basins: Geophysical Journal of the Royal Astronomical Society, **3**, 63–67.

Chai, Y., and W. J. Hinze, 1988, Gravity inversion of an interface above which the density contrast varies exponentially with depth: Geophysics, **53**, 837–845.

Chakravarthi, V., and N. Sundararajan, 2004, Ridge-regression algorithm for gravity inversion of fault structures with variable density: Geophysics, **69**, 1394–1404.

Chakravarthi, V., and N. Sundararajan, 2007, 3D gravity inversion of basement relief — A depth-dependent density approach: Geophysics, **72**, no. 2, I23–I32.

Chappell, A., and N. Kusznir, 2008, An algorithm to calculate the gravity anomaly of sedimentary basins with exponential density-depth relationships: Geophysical Prospecting, **56**, 249–258.

Corbató, C. E., 1965, A least-squares procedure for gravity interpretation: Geophysics, **30**, 228–233.

Cordell, L., 1973, Gravity analysis using an exponential density-depth function — San Jacinto Graben, California: Geophysics, **38**, 684–690.

Davis, P. J., and P. Rabinowitz, 1984, Methods of numerical integration, 2nd ed.: Academic Press, 481–483.

Ferguson, J. F., R. N. Felch, C. L. V. Aiken, J. S. Oldow, and H. Dockery, 1988, Models of the Bouguer gravity and geologic structure at Yucca Flat, Nevada: Geophysics, **53**, 231–244.

García-Abdeslem, J., 1992, Gravitational attraction of a rectangular prism with depth-dependent density: Geophysics, **57**, 470–473.

García-Abdeslem, J., J. M. Romo, E. Gómez-Treviño, J. Ramírez-Hernández, F. J. Esparza-Hernández, and C. F. Flores-Luna, 2005, A constrained 2D gravity model of the Sebastián Vizcaíno Basin, Baja California Sur, Mexico: Geophysical Prospecting, **53**, 755–765.

Guspí, F., 1990, General 2D gravity inversion with density contrast varying with depth: Geoexploration, **26**, 253–265.

Hansen, R. O., 1999, An analytical expression for the gravity field of a polyhedral body with linearly varying density: Geophysics, **64**, 75–77.

Holstein, H., 2003, Gravimagnetic anomaly formulas for polyhedra of spatially linear media: Geophysics, **68**, 157–167.

Holstein, H., and B. Ketteridge, 1996, Gravimetric analysis of uniform polyhedra: Geophysics, **61**, 357–364.

Hubbert, M. K., 1948, A line-integral method of computing the gravimetric effects of two-dimensional masses: Geophysics, **13**, 215–225.

Litinsky, V. A., 1989, Concept of effective density: Key to gravity depth determinations for sedimentary basins: Geophysics, **54**, 1474–1482.

Murthy, I. V. R., and D. B. Rao, 1979, Gravity anomalies of two-dimensional bodies of irregular cross-section with density contrast varying with depth: Geophysics, **44**, 1525–1530.

Pohánka, V., 1988, Optimum expression for computation of the gravity field of a homogeneous polyhedral body: Geophysical Prospecting, **36**, 733–751.

———, 1998, Optimum expression for computation of the gravity field of a polyhedral body with linearly increasing density: Geophysical Prospecting, **46**, 391–404.

Rao, C. V., V. Chakravarthi, and M. L. Raju, 1994, Forward modeling: Gravity anomalies of two-dimensional bodies of arbitrary shape with hyperbolic and parabolic density functions: Computers and Geosciences, **20**, 873–880.

Rao, D. B., 1986, Modeling of sedimentary basins from gravity anomalies with variable density contrast: Geophysical Journal of the Royal Astronomical Society, **84**, 207–212.

Rao, D. B., M. J. Prakash, and N. Ramesh Babu, 1990, 3D and $2\frac{1}{2}$ D modeling of gravity anomalies with variable density contrast: Geophysical Prospecting, **38**, 411–422.

Silva, J. B. C., D. C. L. Costa, and V. C. F. Barbosa, 2006, Gravity inversion of basement relief and estimation of density contrast variation with depth: Geophysics, **71**, no. 5, J51–J58.

Talwani, M., J. L. Worzel, and M. Landisman, 1959, Rapid gravity computations for two-dimensional bodies with application to the Mendocino submarine fracture zone: Journal of Geophysical Research, **64**, 49–59.

Zhang, J., B. Zhong, X. Zhou, and Y. Dai, 2001, Gravity anomalies of 2-D bodies with variable density contrast: Geophysics, **66**, 809–813.

Zhou, X., S. Li, and K. Stamnes, 2003, Geometrical-optics code for computing the optical properties of large dielectric spheres: Applied Optics, **42**, 4295–4306.